IEEE Access
Multidisciplinary ⋮ Rapid Review ⋮ Open Access Journal

Received 29 January 2024, accepted 5 February 2024, date of publication 21 February 2024, date of current version 7 March 2024.

Digital Object Identifier 10.1109/ACCESS.2024.3368805

RESEARCH ARTICLE

Research on the Optimal Control Timing of ZVS-QSW

JIAN YU, (Member, IEEE), LE ZHOU, (Student Member, IEEE), RENHUI SHEN, (Student Member, IEEE), ZHIYUAN SHI, (Student Member, IEEE), AND AOHUI NIU, (Student Member, IEEE)

School of Automation and Software Engineering, Shanxi University, Taiyuan 030000, China

Corresponding author: Jian Yu (yujian15@sxu.edu.cn)

ABSTRACT This article introduces a research method aimed at achieving optimal control timing for the zero-voltage quasi-square wave switch (ZVS-QSW) in a silicon carbide buck converter across a wide range. The method establishes the correlation function between optimal control timing parameters and load current through composite segmented curve fitting to the plane of the ZVS-QSW state over the entire operating range. It also compensates for the charge change on the filter capacitor to determine the load current at the corresponding operating point. By collecting the input/output voltages and load currents and substituting them into the correlation function, the optimal timing parameters for achieving ZVS-QSW can be determined online. The proposed method is validated on a silicon carbide buck converter prototype with an input voltage of 400 V. ZVS-QSW can be achieved in the conversion ratio range of 0.1-0.9. Consequently, the proposed method not only reduces the difficulty of inductance current measurement but also simplifies and visualizes the timing control of the converter.

INDEX TERMS Curve fitting, digital control, quasi-square wave, silicon carbide, zero-voltage switching.

I. INTRODUCTION

Zero-voltage switching quasi-square wave (ZVS-QSW) operation in pulsewidth-modulated dc–dc converters is a well-established method for mitigating turn-ON switching losses, because of the constant-frequency operation with low voltage stresses and relatively low current stresses on active devices [1], [2]. The ZVS-QSW operation is illustrated in Fig. 1 for a buck converter switching cell shown in Fig. 1(a). This approach increases the inductor current ripple such that a sufficiently negative excursion of the current results in a soft zero-voltage transition between the turn-OFF of the synchronous rectifier (SR) switch and the turn-ON of the main switch [3]. These losses can be minimized by optimally setting the negative current during t_{sr} resulting in minimum-conduction ZVS-QSW operation seen in Fig. 1(b). The amount of negative current required depends on the converter input and output voltages [4].

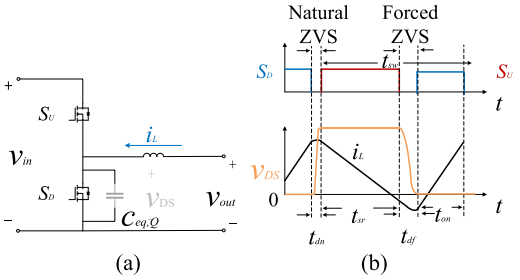

FIGURE 1. (a) Buck converter switching cell. (b) ZVS-QSW operating waveform where the converter realizes ZVS with higher conduction loss losses.

In response to changing operating conditions, these timing parameters must be adjusted online to maintain minimum-conduction ZVS-QSW operation, consequently optimizing converter efficiency over its full operating range.

Online efficiency optimization strategies, in response to changing operating conditions, typically rely on digital implementations. Lookup-table-based approaches that adjust

The associate editor coordinating the review of this manuscript and approving it for publication was Francesco G. Della Corte.

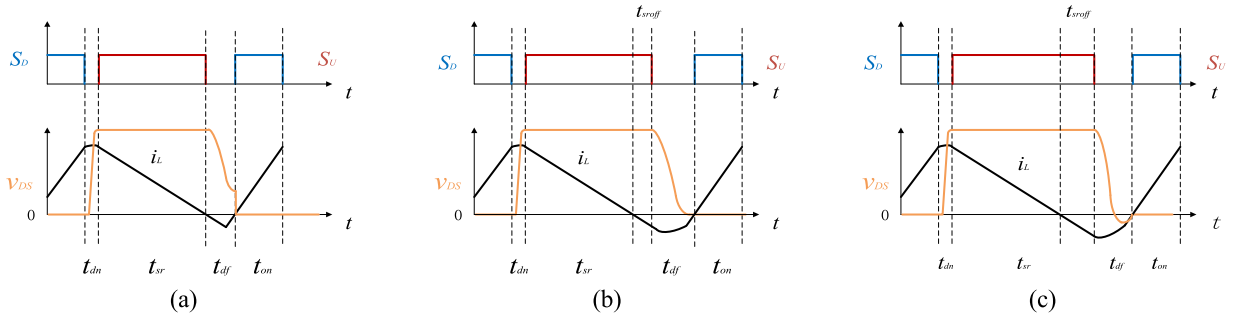

FIGURE 2. Operating waveform in (a) t_{sroff} < desirable value (b) t_{sroff} = desirable value (c) t_{sroff} > desirable value.

switching frequencies and operational modes based on theoretically or empirically determined table entries for a given operating condition are adopted in [5] and [6]. In applications where both the input/output voltages and converter power levels must vary, the table dimensions grow, increasing storage requirements and complexity. The approach in [5], [7], [8], [9], [10], [11], [12], and [13] aims to reduce the computational complexity by fixing one parameter, such as peak SR shutdown current, dead time or frequency, etc., and then adjusting the rest of the parameters by on-line calculations with known conditions, which results in the converter to satisfy the ZVS-QSW operation only in specific ranges, and the switching tubes can only be operated in the hard-switched or suboptimal ZVS operation mode in other ranges. Recently, a research method has been proposed in [4] to realize a wide range of minimum conduction ZVS-QSW operation by adjusting the converter switching frequency and enforcing the zero-voltage dead time online. However, due to the difficulty in measuring the inductor current and the high order of the fitted surface, the computational procedure of this method is complicated and the results are not accurate enough.

The research method proposed in this article for optimal control timing of ZVS-QSW involves obtaining the correlation function between optimal control timing parameters and load current. This is achieved through composite segmented curve fitting to the ZVS-QSW state plane across the entire operating range, along with compensating for the charge change on the filter capacitor to determine the load current at the corresponding operating point. Therefore, this method directly correlates control timing with the output-side current, reducing the complexity of current measurement and parameter calculation. This simplifies and visualizes the timing control strategy.

This article is organized as follows. Section II examines the optimal timing parameter conditions necessary to achieve ZVS-QSW operation through the state plane, deriving formulas for optimal timing parameters in relation to the average current. In Section III, analytical models of the optimal time parameters for each operating point, considering the inductor average current and conversion ratio, are developed. The section also discusses the implementation details of function fitting using the formulas derived in Section II. Section IV establishes the connection between optimal time parameters and load current by overlaying a charge on the filter capacitor. It then briefly outlines the system control block diagram. Section V validates the feasibility and accuracy of the research strategy through simulation tools and experiments, respectively. Finally, Section VI provides a summary of the article.

II. ZVS-QSW CONTROL CONDITION ANALYSIS AND FORMULA DERIVATION

Before developing the analytical models and the resulting fit-functions from the solutions, it is helpful to inspect the trajectory of the optimal timing parameters for variation in each of the converter operating conditions. Since the optimal timing parameters strongly depend on the conversion ratio K [4], in this section, the control conditions for achieving ZVS-QSW in Buck circuits operating at two conversion ratio modes, $K \leq 0.5$ and $K > 0.5$, will be analyzed by the state-plane method. The four timing parameters $t_{on}, t_{dn}, t_{sr}, t_{df}$, and the switching cycle TSW are derived, and finally, the average inductor current i_{Lavg} is obtained.

A. CONVERSION RATIO K>0.5

The waveforms of the buck circuit operation under different control timing conditions are shown in Fig. 2, where i_L is the inductor current and v_{DS} is the voltage across the switching tube S_D. The state plan of the resonance process corresponding to the voltage between the inductor current and the switching parasitic capacitance is shown in Fig. 3, The horizontal coordinate of the state plane is the voltage v_{DS} across the switching tube S_D and the vertical coordinate is the product of the inductor current and the characteristic impedance $i_L \cdot z_n$.

As seen in Fig. 3, the resonant interval can be divided into two stages: ''natural'' resonant interval and ''forced'' resonant interval. For ''natural'' resonant interval, since the radius of the resonance circle $R = v_{out}$ the conversion ratio $K > 0.5$ and $v_{in} - v_{out} < v_{out}$, the resonance process is sufficient for SU zero voltage conduction. The t_{sroff} in Fig. 2 is defined as the time that the inductor current continues to conduct after crossing the zero point. Fig. 3(a) shows the state plan of $t_{sroff} = 0$, at the beginning of resonance the inductor

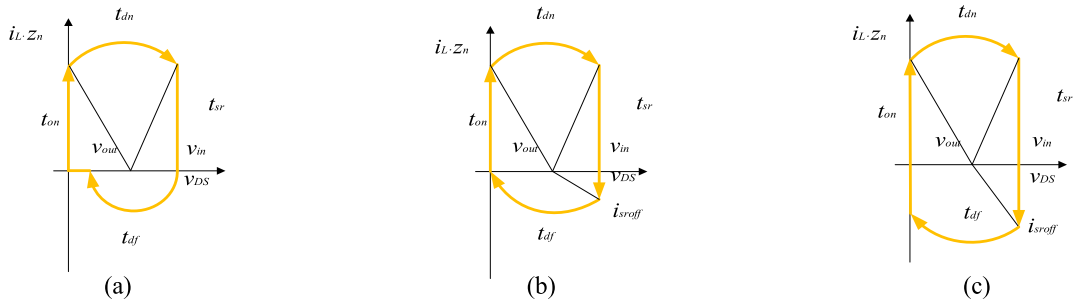

FIGURE 3. State-plan in (a) t_{sroff} < desirable value t_{sroff} = desirable value (c) t_{sroff} > desirable value.

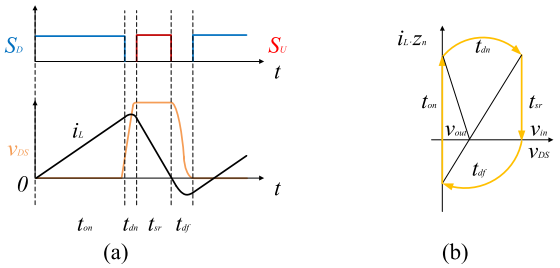

FIGURE 4. (a) Operating waveform in conversion ratio $K \leq 0.5$ (b) Operating waveform in conversion ratio $K \leq 0.5$.

current $i_L = 0$ and the radius of the resonance circle $R < v_{out}$, so the resonance process is sufficient for S_D operates in the hard conduction state, and the resonance waveform of v_{DS} and i_L is shown in Fig. 2(a). Fig. 3(b) shows the state plan of the t_{sroff} = *desirable value*, at the beginning of resonance the inductor current i_L = *desirable value* and the radius of the resonance circle $R = v_{out}$, so the resonance process is sufficient for S_D operates in the zero voltage conduction, and the resonance waveform of v_{DS} and i_L is shown in Fig. 2(b). Fig. 3(c) shows the state plan of the t_{sroff} > *desirable value*, at the beginning of resonance the inductor current i_L > *desirable value* and the radius of the resonance circle $R = v_{out}$, when v_{DS} reaches zero, there is still a negative current in the inductor, causing unnecessary losses and the resonance waveform of v_{DS} and i_L is shown in Fig. 2(c). Calculation of the optimal switching control timing at switching ratios $K > 0.5$ requires the addition of a negative compensation current time t_{sroff} based on the input/output voltages versus the peak inductor current after the synchronous rectification time t_{sr}.

B. CONVERSION RATIO K ≤ 0.5

The corresponding waveforms for the case of conversion ratio $K \leq 0.5$ are shown in Fig. 4(a), and the phase planes of the resonance process of the inductor current and the voltage between the switching parasitic capacitance are shown in Fig. 4(b), and the two phases of the resonance process of the natural commutation and the forced commutation are able to satisfy the switching tubes to realize the ZVS conduction.

C. DERIVATION OF FORMULA

The control conditions for the realization of the converter ZVS-QSW and the corresponding problems need to be solved have been analyzed and presented in detail. Next, using the example of a Buck circuit operating at a conversion ratio $K > 0.5$, the equations for the control time parameters to achieve ZVS-QSW and the corresponding equations for the average current are derived from the state plane.

The calculation method proposed in this strategy is derived from the operating waveform graphs and state planes under the optimal control timing conditions in Fig. 5. Firstly, determining the peak inductor current i_{Lpk} as the intermediate variable i_1, at the end of the natural commutation, the inductor current is i_2, using the natural commutator resonance circle radius R_n to obtain the equation

$$i_1^2 \cdot z_n^2 + v_H^2 = i_2^2 \cdot z_n^2 + v_L^2, \tag{1}$$

where $v_L = v_{in} \cdot K = v_{in}$, $v_H = v_{in} - v_L$, $z_n = \sqrt{L/2C_{otr}}$, L is the value of the inductance, C_{otr} is the output parasitic capacitance of the switching tube, and thus derive

$$i_2^2 = i_1^2 + \frac{(v_L^2 - v_H^2)}{z_n^2}, \tag{2}$$

using the radius of the "forced" resonance circle R_f as an intermediate variable, the following equation is given

$$i_r^2 \cdot z_n^2 + v_L^2 = v_H^2, \tag{3}$$

this results in an inductive negative compensation current

$$i_r^2 = \frac{v_L^2 - v_H^2}{z_n^2}, \tag{4}$$

substituting into Eq. (2), we can get

$$i_2^2 = i_1^2 + i_r^2, \tag{5}$$

for "natural" resonance angles φ_n

$$\varphi_n = \pi - a\cos\left(\frac{v_L}{\sqrt{i_1^2 z_n^2 + v_L^2}}\right) - a\cos\left(\frac{v_H}{\sqrt{i_1^2 z_n^2 + v_L^2}}\right), \tag{6}$$

for "forced" resonance angles φ_f

$$\varphi_f = \pi - a\cos\left(\frac{v_H}{v_L}\right), \tag{7}$$

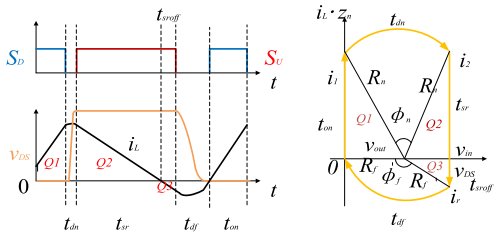

FIGURE 5. (a) Waveform of optimal control timing operation in conversion ratio $K > 0.5$ (b) Optimal Control Timing State Plan in conversion ratio $K > 0.5$.

for the resonant angular frequency ω_n

$$\omega_n = \frac{1}{\sqrt{2LC_{otr}}}, \tag{8}$$

thus we can deduce that

$$t_{on} = \frac{i_1 L}{v_L}, \tag{9}$$

$$t_{dn} = \frac{\varphi_n}{\omega_n}, \tag{10}$$

$$t_{sr} = \frac{(i_2 + i_r) \cdot L}{v_H} = \frac{(\sqrt{i_1^2 + i_r^2} + i_r) \cdot L}{v_H}, \tag{11}$$

$$t_{df} = \frac{\varphi_f}{\omega_n}, \tag{12}$$

in turn, we can derive the switching cycle

$$TSW = t_{on} + t_{dn} + t_{sr} + t_{df}, \tag{13}$$

The positive and negative charges of the ''natural'' and ''forced'' commutation processes cancel each other out, thus the total charge of one switching cycle is equal to the sum of $\mathbf{Q}_1$, $\mathbf{Q}_2$, $\mathbf{Q}_3$ and in Fig. 5(a), where $\mathbf{Q}_1 = i_1^2 L/2v_L$, $\mathbf{Q}_2 = i_2^2 L/2v_H$, $\mathbf{Q}_3 = ir^2 L/2v_H$, combined with formula (5), it can be deduced that

$$\mathbf{Q} = \frac{i_1^2 L}{2} \cdot \left(\frac{1}{v_L} + \frac{1}{v_H}\right) = \frac{i_1^2 L}{2v_{in}} \cdot \frac{1}{k(1-k)}, \tag{14}$$

where k is the conversion ratio and finally we get the average inductor current in one cycle

$$i_{Lavg} = \frac{\mathbf{Q}}{t_{on} + t_{dn} + t_{sr} + t_{df}}. \tag{15}$$

III. MODELING AND FUNCTION FITTING OF OPTIMAL CONTROL TIMING PARAMETERS AT VARIOUS OPERATING POINTS

Section II has analyzed the control conditions for achieving ZVS-QSW in the converter across the full operating range. It derived the optimal control timing and the equation for the average inductor current. This serves as a data source for the subsequent analysis of the control timing trends and function fitting to achieve ZVS-QSW at each operating point.

A. MATHEMATICAL MODELING OF OPTIMAL TIME PARAMETERS

This proposed strategy generates uniform independent variable input voltage v_{in}(200-400 V), output voltage v_{out}(0.005·v_{in}-1·v_{in}) and inductor average current i_{Lavg} (0-60 A) by mathematical tools. The next step is the calculation of the dependent time parameters t_{on}, t_{dn}, t_{sr}, t_{df} and the inductor average current i_{Lavg}, from the second section, it can be seen that this research strategy uses two different control timing calculations for conversion ratios $K \leq 0.5$ and $K > 0.5$, respectively. So for the time parameter also two separate sets of formulas were used to calculate the obtained. Fig. 6 shows the parametric modeling of the time parameters t_{on}, t_{dn}, t_{sr}, computed from the conversion ratio K and the peak inductor current i_{Lpk}, for conversion ratios $K \leq 0.5$ and $K > 0.5$, respectively, in a specific range. However, the value of the time parameter t_{sr} is only related to the conversion ratio K. Fig.7 shows the parametric model of the time parameter t_{sr} for conversion ratios $K \leq 0.5$ and $K > 0.5$.

Fig. 6 (a, b, c, d) and 7 (a, b, c, d) show the model surface plots of the optimal time parameters (t_{on}, t_{dn}, t_{sr}, t_{df}) for the independent variable input voltage v_{in} varying from 200 to 400 V and the inductor average current i_{Lavg} varying from 5 A to 50 A for the conversion ratios $K > 0.5$ and $K \leq 0.5$, respectively.

From this, we can calculate the corresponding optimal control timing parameters t_{on}, t_{dn}, t_{sr}, t_{df} for conversion ratio K and peak inductor current i_{Lpk} from the resonant state phase plane. However, the challenge in measuring the peak inductor current renders it impossible to calculate the time parameter required to achieve the transition of the switching tubes from ZVS to QSW in a wide range mode, using the conversion ratio and peak inductor current to meet the requirements of the wide range mode. Fortunately, we also find that the average inductor current i_{Lavg} calculated at the corresponding conversion ratio K and peak inductor current i_{Lpk} is fixed, this means that the time parameters for realizing the switching tubes ZVS-QSW at the corresponding conversion ratio K and inductor average current i_{Lavg} are fixed, and theoretically we can derive the corresponding time parameters from the specific conversion ratio K and the inductor average current i_{Lavg}. However, this backpropagation process is very difficult and the derived function is very cumbersome. Therefore, this article proposes a method to fit the four time parameters realizing the switching tubes ZVS-QSW with the conversion ratio K and the inductor average current i_{Lavg} as a function of the load output voltage v_{out} and the inductor average current i_{Lavg}, respectively.

B. FUNCTION FITTING

If the time parameters t_{on}, t_{dn}, t_{sr} are fitted directly to the binary polynomials of the conversion ratio K and the average inductor current i_{Lavg} at a constant input voltage of 400 V, the fitting function will be very complicated and less accurate. Therefore, this proposed strategy uses a double fitting

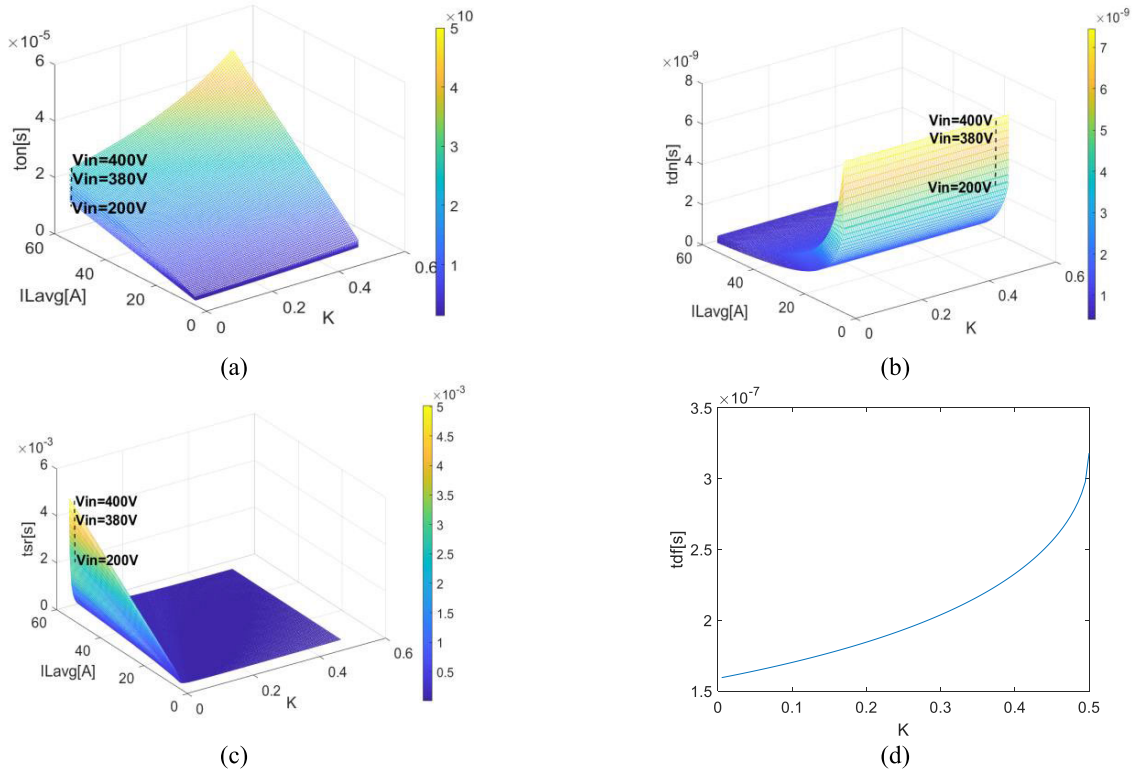

FIGURE 6. Analytical modeling of time parameters with inductor average current and conversion ratio K for conversion ratio $K > 0.5$. (a)The analytic model of t_{on}. (b) The analytic model of t_{dn}. (c) The analytic model of t_{sr}. (d) The analytic model of t_{df}.

approach, where the time parameters t_{on}, t_{dn}, and t_{sr} are first fitted to the inductor average current i_{Lavg} in a low-order linear fashion, and then the coefficients of the primary fitting function are fitted to the conversion ratio K in a secondary fashion, which ultimately yields the composite function of the optimal time parameters with respect to the buck ratio K and the inductor average current i_{Lavg}.

1) PRIMARY FUNCTION FITTING

As an example of the optimal time parameter t_{on}, Fig. 8 shows a plot of the time parameter t_{on} fitted as a function of the average inductor current at an input voltage of 400 V and a conversion ratio of 0.6. The curve of the time parameter t_{on} versus the inductor average current is fitted to obtain a 3rd order linear function over the range of the inductor average current of (0-0.5A)

$$f_1(x) = p_{11}x^3 + p_{12}x^2 + p_{13}x + p_{14}, \tag{16}$$

where $p_{11} = 8.861e\text{-}7$, $p_{12} = -8.933e\text{-}7$, $p_{13} = 5.911e\text{-}7$, $p_{14} = 2.393e\text{-}7$○

The curve of the time parameter ton versus the inductor average current i_{Lavg} is fitted to obtain a 3rd order linear function over the range of the inductor average current i_{Lavg} of (0.5-4.5 A)

$$f_2(x) = p_{21}x^3 + p_{22}x^2 + p_{23}x + p_{24}, \tag{17}$$

where $p_{21} = 2.589e\text{-}10$, $p_{22} = -3022e\text{-}9$, $p_{23} = 2.641e\text{-}7$, $p_{24} = 7.723e\text{-}8$.

Following the above method, the optimal time parameters t_{on}, t_{dn}, and t_{sr} are obtained as more accurate linear 3rd order functions in a suitable range of inductor average current i_{Lavg}, respectively. That will also lead to another question, i.e., how will the segmentation point of the inductor average current i_{Lavg} change as the conversion ratio K changes? Fortunately, by comparing the curves of the time parameters t_{on}, t_{dn}, and t_{sr} with the average inductor current i_{Lavg} for different conversion ratios, it is found that the curves follow the same trend i.e., the segmentation points are the same.

2) SECONDARY FUNCTION FITTING

The strategy proposed in this article obtains multiple sets of primary segmented functions for the variation of the time parameters t_{on}, t_{dn}, and t_{sr} with the inductor average current i_{Lavg} at an input voltage of 400 V and a conversion ratio K(0-1), respectively, by primary function fitting. And then the coefficients of each primary function with the conversion ratio K are subjected to secondary function fitting. Fig. 9 shows the segmented fitting curves of the coefficients $p11$ of the primary fitting function of t_{on} and the corresponding average current i_{Lavg} as a function of the conversion ratio K for an input voltage of 400 V and a range of variation of the conversion ratio K(0-1).

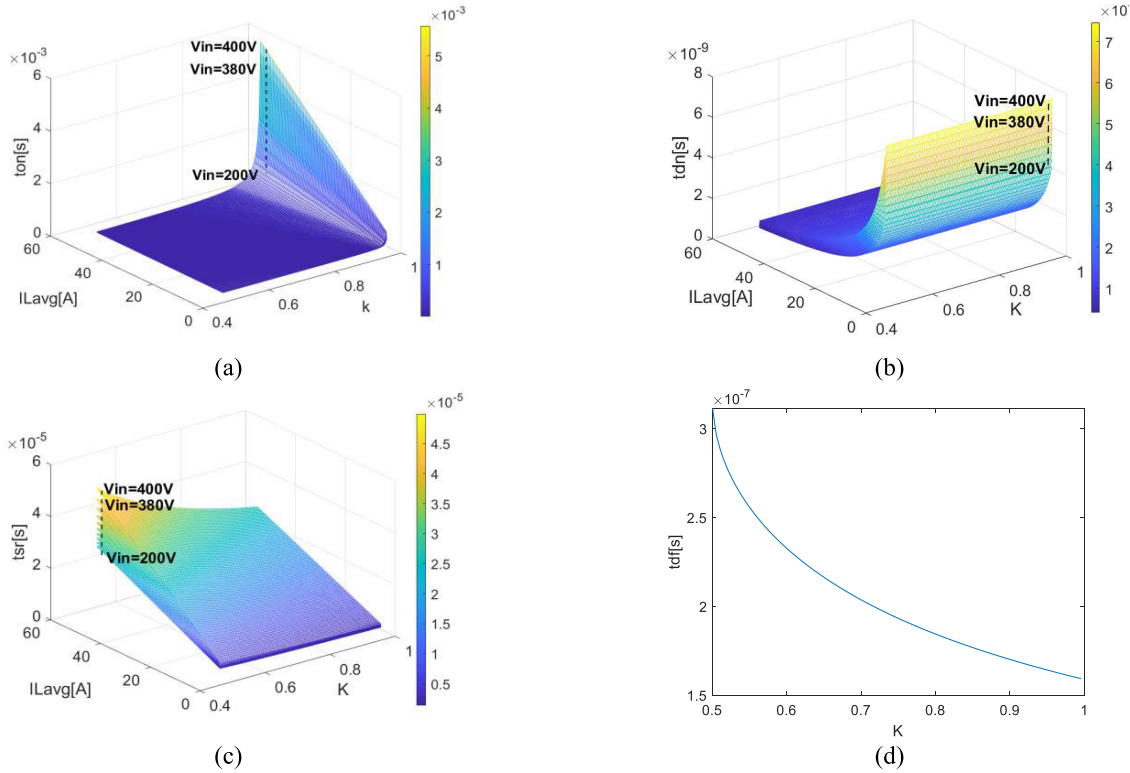

FIGURE 7. Analytical modeling of time parameters with inductor average current and conversion ratio K for conversion ratio $K \leq 0.5$. (a)The analytic model of t_{on}. (b) The analytic model of t_{dn}. (c) The analytic model of t_{sr}. (d) The analytic model of t_{df}.

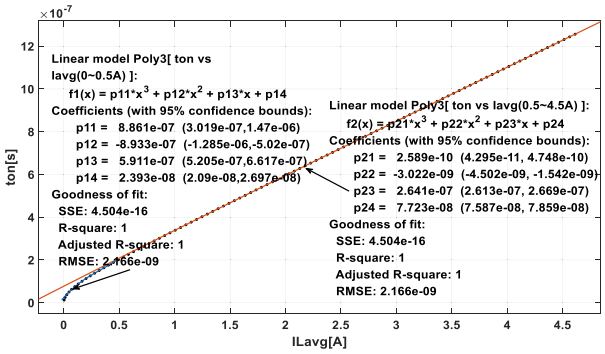

FIGURE 8. Plot of the time parameter ton fitted as a function of the average inductor current i_{Lavg} for an input voltage of 400 V and a conversion ratio K of 0.6.

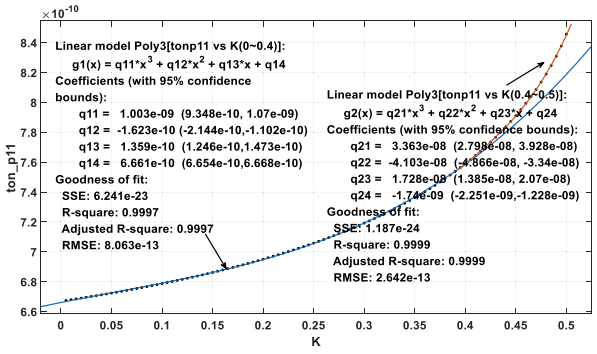

FIGURE 9. Plot of the segmented fit of the coefficients $p11$ of the primary fitting function of ton as a function of the transition ratio K (0-(1).

The curve of the coefficients $p11$ of t_{on}'s primary fitted function versus the conversion ratio K is fitted to obtain a 3rd order linear function in the range of the conversion ratio K of (0-0.4)

$$g_1(x) = q_{11}x^3 + q_{12}x^2 + q_{13}x + q_{14}, \tag{18}$$

where $q_{11} = 8.861e\text{-}7$, $q_{12} = -8.933e\text{-}7$, $q_{13} = 5.911e\text{-}7$, $q_{14} = 2.393e\text{-}7$.

The curve of the coefficients $p11$ of t_{on}'s primary fitted function versus the conversion ratio K is fitted to obtain a 3rd order linear function in the range of the conversion ratio K of (0.4-0.5)

$$g_2(x) = q_{21}x^3 + q_{22}x^2 + q_{23}x + q_{24} \tag{19}$$

where $q_{21} = 8.861e\text{-}7$, $q_{22} = -8.933e\text{-}7$, $q_{23} = 5.911e\text{-}7$, $q_{24} = 2.393e\text{-}7$.

According to this method more accurate linear 3rd order functions with coefficients $p11 - p14$ of the primary fitting functions of the optimal time parameters t_{on}, t_{dn}, t_{sr} can be obtained in the range of suitable conversion ratios K.

The optimal time parameter t_{df} is only related to the conversion ratio K. Therefore, the segmented fitting function of

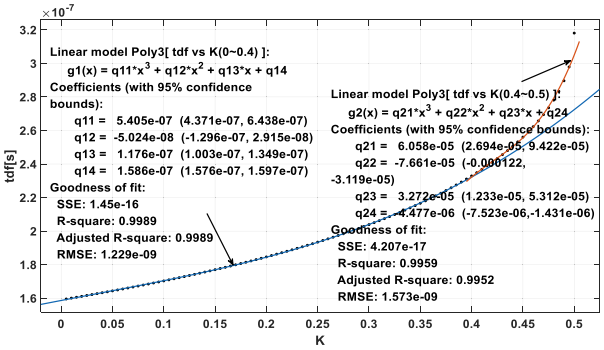

FIGURE 10. Plot of the segmental fit of t_{df} to the conversion ratio K (0-0.5).

the "forced" resonant interval t_{df} versus the conversion ratio K is shown in Fig. 10.

The curve of the time parameter t_{df} versus the conversion ratio K is fitted to obtain a 3rd order linear function in the range of conversion ratios K of (0-0.4)

$$g_1(x) = q_{11}x^3 + q_{12}x^2 + q_{13}x + q_{14}, \tag{20}$$

where $q_{11} = 5.405e\text{-}7$, $q_{12} = -5.024e\text{-}7$, $q_{13} = 1.176e\text{-}7$, $q_{14} = 1.586e\text{-}7$.

The curve of the time parameter t_{df} versus the conversion ratio K is fitted to obtain a 3rd order linear function in the range of conversion ratios K of (0.4-0.5)

$$g_2(x) = q_{21}x^3 + q_{22}x^2 + q_{23}x + q_{24}, \tag{21}$$

where $q_{21} = 6.058e\text{-}7$, $q_{22} = -7.661e\text{-}7$, $q_{23} = 3.272e\text{-}7$, $q_{24} = -4.477e\text{-}7$.

C. CALIBRATION OF THE FITTING FUNCTION

The strategy proposed in this article uses primary and secondary third-order function fitting in order to reduce the complexity of a single computation and to improve the accuracy, so the relative error between the curve-fit timing parameters and the analytical values is a matter of great concern. The accuracy of the fitted function is verified by taking the optimum control time parameters of ZVS-QSW realized at the operating points with input voltage of 400 V and conversion ratio K in the range of (0.5-1) as an example, and the comparison of the curve-fit values with the analytical values is plotted in Fig. 11(a, b, c, d), where the curve-fit values of the individual operating points are compared with the analytical values as shown in Table 1.

The analytical values of different operating points randomly selected from the optimal time parameter control charts were analyzed with the curve-fit values, and the relative errors did not exceed 5%, which is enough to have verified that the accuracy of the fitted function is very satisfactory.

Due to the fact that two different ways of fitting functions are used in this fitting for conversion ratios $K > 0.5$ and conversion ratios $K \leq 0.5$, and in order to improve the accuracy of the fitting function and at the same time to reduce

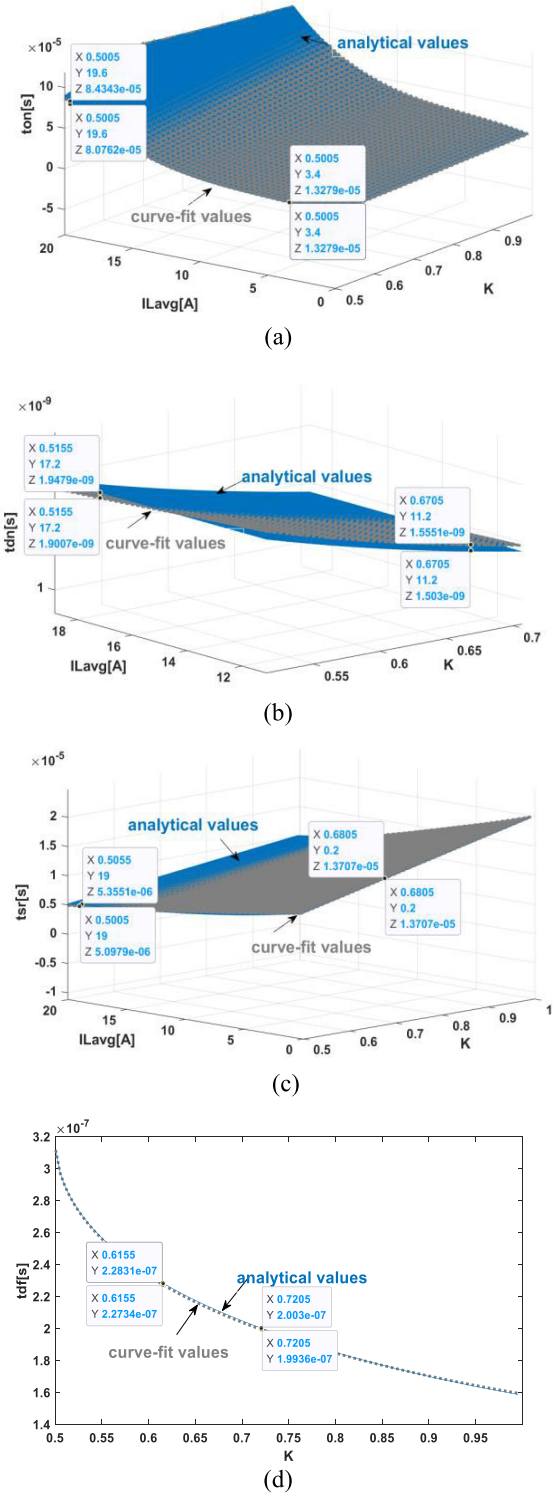

FIGURE 11. (a) Comparison plot of analytical vs. curve fit values for t_{on}. (b) Comparison plot of analytical vs. curve fit values for t_{dn}. (c) Comparison plot of analytical vs. curve fit values for t_{sr}. (d) Comparison plot of analytical vs. curve fit values for t_{df}.

the order of the fitting function, segmented fitting is also carried out at different average current points. Therefore, in the full range mode of operation, the segmented fitting

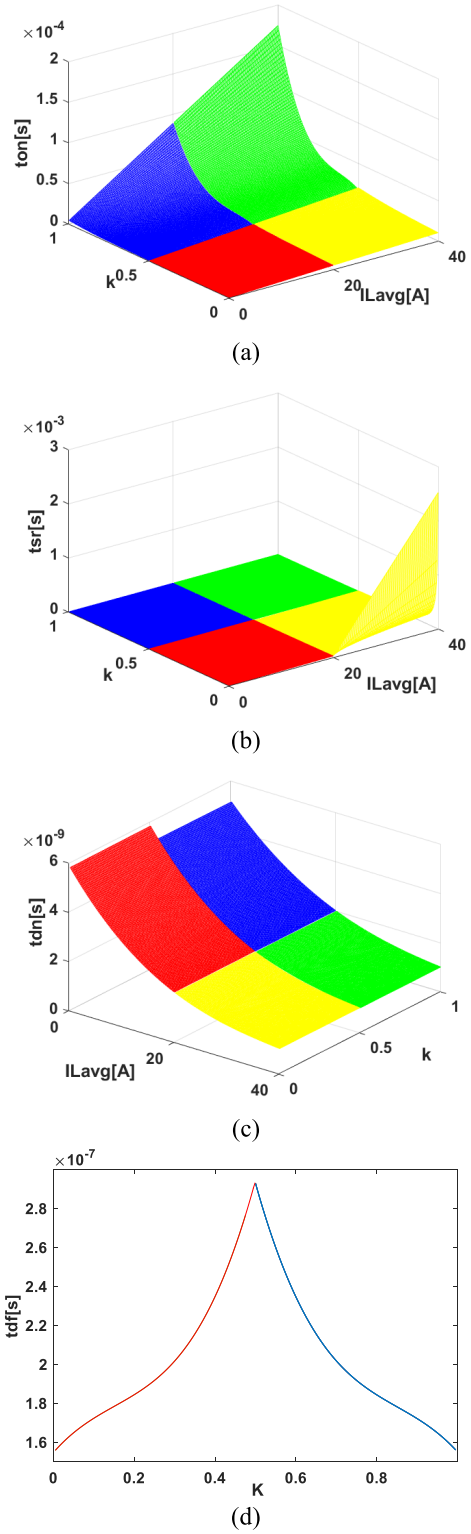

FIGURE 12. (a) t_{on} fits the surface map over the full range. (b) t_{dn} fits the surface map over the full range. (c) t_{sr} fits the surface map over the full range. (d) t_{df} fits the surface map over the full range.

function should be very approximate at the exchange point in order to ensure the stability of the output.

TABLE 1. Comparison of curve-fit and analytical values.

Time Parameter	Operating point	Analytical values[s]	Curve-fit values[s]
t_{on}	K=0.5005/I_{Lavg}=19.8 A	8.4343e-5	8.0762e-5
	K=0.5005/I_{Lavg}=3.4 A	1.3279e-5	1.3279e-5
t_{dn}	K=0.5155/I_{Lavg}=17.2 A	1.9479e-9	1.503e-9
	K=0.6705/I_{Lavg}=11.2 A	1.5551e-9	1.9007e-9
t_{sr}	K=0.5055/I_{Lavg}=19 A	5.3551e-6	5.0979e-6
	K=0.6805/I_{Lavg}=0.2 A	1.3707e-5	1.3707e-5
t_{df}	K=0.6155	2.2831e-7	2.2734e-7
	K=0.7205	2.003e-7	1.9936e-7

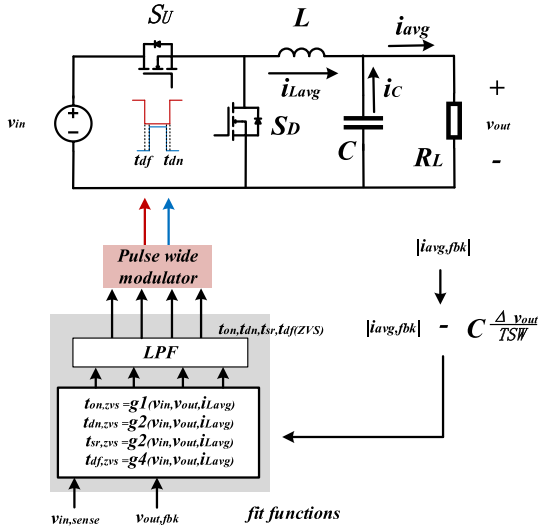

FIGURE 13. ZVS_QSW Control Structure Block Diagram.

The surface plots of the wide operating ranges of the four time parameters calculated by fitting the obtained segmented functions are shown in Fig. 12, segmented functions are approximately coincident wherever they meet over the full operating range.

IV. CHARGE SUPERPOSITION ON FILTER CAPACITORS

With the fitting method in Section III, we obtain the fitting functions of each of the four time parameters with respect to the load output/input voltage and the inductor average current i_{Lavg}. Through the fitting method in Section III, we obtain the fitting functions of the four time parameters with the output/input voltages and the average inductor current i_{Lavg}, respectively. However, this method is difficult and susceptible to disturbances in measurement of the inductor current in the high-frequency and output-voltage-variable operating modes.

Fig. 13 shows the block diagram of the control strategy structure proposed in this article to realize ZVS-QSW. This strategy removes the current I_c generated by the change of charge on the filter capacitor from the load output average current i_{avg} to obtain the corresponding inductor average current i_{Lavg}, the optimal time parameters are then calculated by bringing them together with the output and input voltages into the fitting function obtained in Chapter III. The predicted optimal timing parameters are applied to the

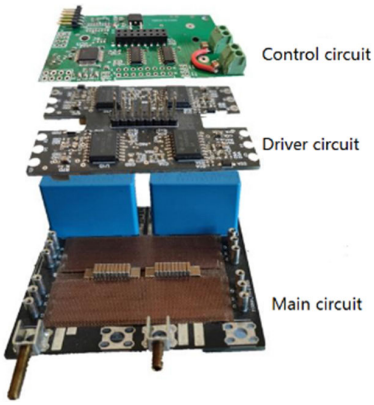

FIGURE 14. SiC-based buck converter prototype.

TABLE 2. Boost converter parameter.

Parameter	Value\Specifications
Input voltage, v_{in}	400V
Output voltage, v_{out}	50V-300V
Isolated Driver	ISO5852SDWR
Half-Bridge module	C3M0075120K
inductor	50uH
Controller	STM32f334C8T6

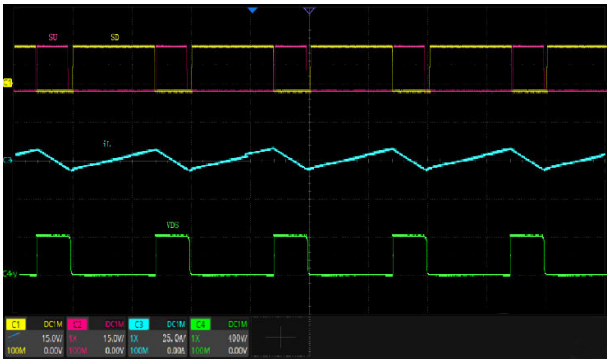

FIGURE 15. Waveforms of the gate control level as well as the voltage VDS across the lower tube and the sense average current I_{Lavg} for an input voltage of 400 V and an output voltage of 100 V.

pulse-width modulator (PWM) through low-pass filters to ensure smooth transitions as the operating conditions change. The converter eventually settles at timing parameters that achieve ZVS-QSW for a given operating point.

V. EXPERIMENTAL VALIDATION

The previous section of this article fitted a multivariate linear function of the optimal control timing over a wide operating range and converted the computational factor inductor-averaged current i_{Lavg} to the load output current i_{avg} by charge superposition on the filter capacitors. This section verifies that the on-line optimal control timing of the converter demonstrates minimum conduction ZVS-QSW operation over a wide range of conversion ratios and power levels.

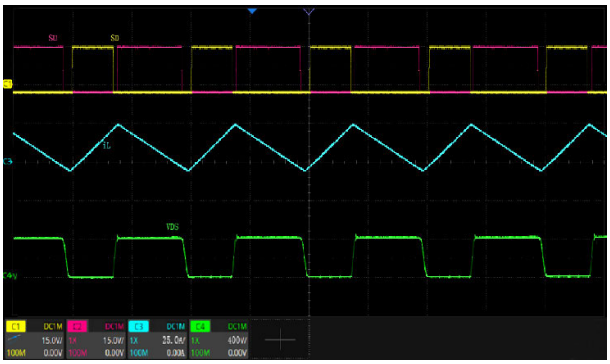

FIGURE 16. Waveforms of the gate control level as well as the voltage VDS across the lower tube and the sense average current I_{Lavg} for an input voltage of 400 V and an output voltage of 240 V.

In order to verify the on-line optimization strategy proposed in this article, the SiC buck converter prototype shown in Fig. 14 is constructed in this experiment, and its relevant parameters are shown in Table 2, and the load is resistive load. After programming the fitting function into the controller, we capture the gate control level as well as the voltage and average inductor current across the downstream tube with an oscilloscope for a gate input voltage of 400 V, and output voltages of 100 V and 240 V. In the captured plots in Figs. 15 and 16, the switching tube all conducts at its terminal voltage $v_{DS} = 0$, i.e., the ZVS-QSW is realized. It can be verified that the optimal control timing study method proposed in this article can realize the ZVS-QSW operation over a wide operating range.

VI. CONCLUSION

Realizing ZVS-QSW operation requires precise adjustment of timing parameters, especially under changing operating conditions. These timing parameters must be adjusted online. In this article, we propose an optimal control timing study method for ZVS-QSW. This method involves composite segmented curve fitting to the ZVS-QSW state plane over the full operating range. It also compensates for the charge change on the filter capacitor to obtain the load current at the corresponding operating point. This approach allows us to establish the correlation function between the optimal control timing parameters and the load current. The control timing is directly linked to the output side current, which reduces the difficulty of current measurement and parameter calculation. This makes the timing control strategy simpler and more visualized. The online optimization method proposed in this article is validated on a SiC buck prototype. The online-tuned timing parameters closely align with the optimal values of the analytical model, enabling ZVS-QSW operation under different operating conditions. The systematic methodology for building the analytical model, the generated curve fitting procedure, and the implementation techniques presented in this article can be applied to other converter topologies.

ACKNOWLEDGMENT

The views and opinions expressed in this article do not necessarily state or reflect those of the Chinese government or any of its agencies. The work presented in this article extends the method presented in [3] and [4] and compensates for charge variations on the filter capacitor linking the optimal control time parameter to the load current. Additional experimental results are provided that the present method can realize ZVS-QSW operation over a wider range of operating conditions.

REFERENCES

[1] X. Chen, J. Xu, and G. Xu, "Hybrid SPS control for ISOP dual-active-bridge converter based on modulated coupled inductor with full load range ZVS and RMS current optimization in DC transformer applications," *IEEE Access*, vol. 10, pp. 131394–131405, 2022, doi: 10.1109/ACCESS.2022.3227965.

[2] D. Neumayr, D. Bortis, and J. W. Kolar, "The essence of the little box challenge—Part A: Key design challenges & solutions," *CPSS Trans. Power Electron. Appl.*, vol. 5, no. 2, pp. 158–179, Jun. 2020, doi: 10.24295/CPSSTPEA.2020.00014.

[3] V. Sankaranarayanan, Y. Gao, R. W. Erickson, and D. Maksimovic, "Online efficiency optimization of a closed-loop controlled SiC-based boost converter," in *Proc. IEEE Appl. Power Electron. Conf. Expo. (APEC)*, Mar. 2020, pp. 285–291.

[4] V. Sankaranarayanan, Y. Gao, R. W. Erickson, and D. Maksimovic, "Online efficiency optimization of a closed-loop controlled SiC-based bidirectional boost converter," *IEEE Trans. Power Electron.*, vol. 37, no. 4, pp. 4008–4021, Apr. 2022, doi: 10.1109/TPEL.2021.3123965.

[5] D. Neumayr, D. Bortis, E. Hatipoglu, J. W. Kolar, and G. Deboy, "Novel efficiency-optimal frequency modulation for high power density DC/AC converter systems," in *Proc. IEEE 3rd Int. Future Energy Electron. Conf. ECCE Asia*, Jun. 2017, pp. 834–839, doi: 10.1109/IFEEC.2017.7992148.

[6] S. H. Kang, D. Maksimovic, and I. Cohen, "Efficiency optimization in digitally controlled flyback DC–DC converters over wide ranges of operating conditions," *IEEE Trans. Power Electron.*, vol. 27, no. 8, pp. 3734–3748, Aug. 2012, doi: 10.1109/TPEL.2012.2186590.

[7] M. C. Lazar and M. P. Shreelakshmi, "Efficient bidirectional DC–DC converter using digital adaptive frequency modulation," in *Proc. IEEE Int. Power Renew. Energy Conf. (IPRECON)*, Sep. 2021, pp. 1–6.

[8] B. Agrawal, L. Zhou, A. Emadi, and M. Preindl, "Variable-frequency critical soft-switching of wide-bandgap devices for efficient high-frequency nonisolated DC–DC converters," *IEEE Trans. Veh. Technol.*, vol. 69, no. 6, pp. 6094–6106, Jun. 2020, doi: 10.1109/TVT.2020.2987028.

[9] T. Konjedic, L. Korosec, M. Truntic, C. Restrepo, M. Rodic, and M. Milanovic, "DCM-based zero-voltage switching control of a bidirectional DC–DC converter with variable switching frequency," *IEEE Trans. Power Electron.*, vol. 31, no. 4, pp. 3273–3288, Apr. 2016, doi: 10.1109/TPEL.2015.2449322.

[10] J.-B. Baek, W.-I. Choi, and B.-H. Cho, "Digital adaptive frequency modulation for bidirectional DC–DC converter," *IEEE Trans. Ind. Electron.*, vol. 60, no. 11, pp. 5167–5176, Nov. 2013, doi: 10.1109/TIE.2012.2224075.

[11] Y.-C. Liu, Y.-L. Syu, N. A. Dung, C. Chen, K.-D. Chen, and K. A. Kim, "High-switching-frequency TCM digital control for bidirectional-interleaved buck converters without phase error for battery charging," *IEEE J. Emerg. Sel. Topics Power Electron.*, vol. 8, no. 3, pp. 2111–2123, Sep. 2020, doi: 10.1109/JESTPE.2019.2954602.

[12] D. Lyu, G. Shi, R. Min, Q. Tong, Q. Zhang, L. Li, and G. Shen, "Extended off-time control for CRM boost converter based on piecewise equivalent capacitance model," *IEEE Access*, vol. 8, pp. 155891–155901, 2020, doi: 10.1109/ACCESS.2020.3019089.

[13] Q. Huang and A. Q. Huang, "Variable frequency average current mode control for ZVS symmetrical dual-buck H-bridge all-GaN inverter," *IEEE J. Emerg. Sel. Topics Power Electron.*, vol. 8, no. 4, pp. 4416–4427, Dec. 2020, doi: 10.1109/JESTPE.2019.2940270.

JIAN YU (Member, IEEE) was born in Taiyuan, Shanxi. He received the B.S. degree in electrical technology from the Department of Electric Power, Sichuan United University (formerly Chengdu University of Science and Technology, now Sichuan University), in July 1995, and the Ph.D. degree in mechatronics engineering from Beijing Institute of Technology, in March 2009. Since 1995, he has been teaching circuits, electronics, and communications. From 2010 to 2012, he was a Postdoctoral Fellow and a Guest Researcher with Beijing University of Aeronautics and Astronautics and the Institute of Electronics, Chinese Academy of Sciences. He is responsible for completing many horizontal research projects. He has published eight scientific articles as the first author and has been authorized two national invention patents and three utility model and appearance patents.

LE ZHOU (Student Member, IEEE) was born in Suzhou, Anhui. He received the B.S. degree from Anhui University of Engineering, in July 2021. From 2021 to 2024, he studied at Shanxi University, majoring in control science and engineering. Since 2017, he has been a longtime researcher in circuits, electronics, and communications. He participated in a number of power electronics horizontal research in graduate school. At undergraduate stage, he participated in the Blue Bridge Cup Competition and won the first prize in the provincial competition and the second prize achievement in the national competition.

RENHUI SHEN (Student Member, IEEE) was born in Chuzhou, Anhui. He received the B.S. degree from the Wanxi College, and the master's degree from the School of Automation and Software, Shanxi University, in 2024. He has participated in many power electronics horizontal research during the graduate studies.

ZHIYUAN SHI (Student Member, IEEE) was born in Handan, Hebei. He received the B.S. degree from Henan University of Technology, in July2021. He has been studying at Shanxi University, since September 2021. His research interest includes power electronics. He is mainly engaged in the research of LCL-type grid-connected inverter control technology with inverter-side current feedback. He has participated in several lateral research of power electronics projects during the postgraduate studies.

AOHUI NIU (Student Member, IEEE) was born in Changzhi, Shanxi. He received the bachelor's degree from Shanxi University, in 2021. He studied control science and engineering at Shanxi University, from 2021 to 2024. Since 2017, he has been studying courses, such as circuits and power electronics for a long time. During the graduate studies, he participated in multiple horizontal research projects in power electronics.